Applied Physics Letters ARTICLE scitation.org/journal/apl

Effective spin injection into the organic semiconductor PTCDA evaluated by a normalization method

Cite as: Appl. Phys. Lett. **121**, 232401 (2022); doi: 10.1063/5.0106446
Submitted: 28 June 2022 · Accepted: 21 November 2022 ·
Published Online: 5 December 2022

Sheng-Yueh Weng,[1] M. Sanjoy Singh,[1,2] Cheng-Feng Hong,[1] Wen-Teng Lin,[1] Po-Hsun Wu,[1] Ssu-Yen Huang,[1] Jauyn Grace Lin,[3] Yu-Hsun Chu,[1] Wen-Chung Chiang,[4] and Minn-Tsong Lin[1,5,6,a)]

AFFILIATIONS

[1]Department of Physics, National Taiwan University, Taipei 10617, Taiwan
[2]Nano Science and Technology Program, Taiwan International Graduate Program, Academia Sinica, Taipei 11529, Taiwan
[3]Center for Condensed Matter Sciences, National Taiwan University, Taipei 10617, Taiwan
[4]Department of Optoelectric Physics, Chinese Culture University, Taipei 11114, Taiwan
[5]Research Center for Applied Sciences, Academia Sinica, Taipei 11529, Taiwan
[6]Institute of Atomic and Molecular Sciences, Academia Sinica, Taipei 10617, Taiwan

[a)]**Author to whom correspondence should be addressed:** mtlin@phys.ntu.edu.tw

ABSTRACT

Studies of spin current injection, transport, and interface control have drawn attention recently for efficient organic spintronic devices. In this study, we apply both spin pumping (SP) and the longitudinal spin Seebeck effect (LSSE) to inject spin currents into a π-conjugated organic semiconductor, perylene-3,4,9,10-tetracarboxylic dianhydride (PTCDA), and characterize injection and transport by measuring inverse spin Hall voltage V_{ISHE} in spin detectors. A normalization factor introduced to SP analysis eliminates a contribution provoked by deviation of spin sources and leads to a more accurate determination of the spin diffusion length in PTCDA. While SP with Permalloy as a spin source is effective in generating detectable V_{ISHE}, the LSSE from yttrium iron garnet shows no convincing sign of spin injection. In addition, spin-flip scattering induced by hybrid states undermining electrical spin injection is negligible in SP. These results are attributed to interfaces between spin sources and PTCDA, indicative of the importance of injection methods and material choices.

Organic semiconductors (OSCs) are growing alternatives to conventional spintronic materials by virtue of their unique properties such as low cost, mechanical flexibility, and, in particular, the weak spin–orbit coupling, which leads to long spin relaxation time,[1] a key property for efficient spin transport. Spin-injection into and spin-transport within OSCs have inspired promising technological applications in the field of organic spintronics. Over the past decades, spin-polarized carriers have been injected into OSCs in spin valves[2] and light emitting diodes[3,4] by bias voltage. Furthermore, microscopic techniques, including two-photon photoemission[5] and a low energy muon spin rotation,[6] have been applied to demonstrate spin injection and transport in OSCs as well. OSCs–metal interfaces also introduce spin-charge conversion by effects such as Rashba spin splitting and cooperative molecular field.[7,8]

However, generation, manipulation, and detection of spin polarization along a vertical direction in a layered structure such as an organic spin valve are challenging with issues ranging from interfacial roughness to material compatibility and conductivity mismatch at an interface, which involves OSCs and other materials.[9–11] One method we have demonstrated in the past to overcome parts of these issues is the insertion of a thin insulating layer at OSC/ferromagnet interfaces, which significantly improves spin injection efficiency and allows spin-polarized carriers to propagate through the OSC spacers.[12–14] Recently, spin pumping (SP) and the spin Seebeck effect have been proposed to effectively inject pure spin currents from ferromagnetic layers into OSC layers as solutions to conductivity mismatch.[15–17] In general, how to effectively generate and inject spin using these techniques is a crucial issue to realistic applications.

In this work, we applied both SP and the longitudinal spin Seebeck effect (LSSE) to inject spin currents into an organic semiconducting layer of perylene-3,4,9,10-tetracarboxylic dianhydride (PTCDA), which has been favorably used in organic thin-film transistors and organic light-emitting diodes due to its planar adhesion and

low surface roughness.[18–20] A platinum (Pt) layer is established adjacent to PTCDA as a spin detector, whereas spin currents induced by SP/LSSE are generated from a Permalloy (Py)/yttrium iron garnet (YIG) layer.[21,22] The injected spin currents propagating through PTCDA from the spin sources would reach Pt and then converted into charge currents by the inverse spin Hall effect (ISHE).[23,24] A normalization factor is introduced to the ISHE voltage (V_{ISHE}) for SP and disposes of deviations from the spin sources. While spin transport from Py through PTCDA agrees with the work of Nishida *et al.*,[25] the induced V_{ISHE} is largely suppressed in YIG-based LSSE systems. We attribute these results to a change of spin mixing conductance and discuss improvements of interfacial issues.

For the SP measurements, 10 nm Pt was grown on $1.5 \times 4\,\mathrm{mm}^2$ clean glass substrates by magnetron sputtering. Afterward, $1.5 \times 3\,\mathrm{mm}^2$ PTCDA with various thickness t was deposited on top of Pt by thermal evaporation and then covered by $1.5\,\mathrm{mm} \times 2\,\mathrm{mm} \times 10\,\mathrm{nm}$ Py. The devices were prepared in UHV with a base pressure of 1×10^{-8} Torr. A growth rate around 1.5 Å/s for PTCDA was certified using an atomic force microscope (AFM). Such deposition rate yields surface roughness of around 1.4 nm for PTCDA on Pt and YIG, of which the AFM images are shown in the supplementary material. In the LSSE measurements, 0.5 mm commercial polycrystalline YIG slabs with a dimension of $2 \times 5\,\mathrm{mm}^2$ function as both substrates and spin sources. The ferrimagnetic insulator YIG has been widely used as substrates to get rid of the unwanted anomalous Nernst effect. The same procedures are used to grow PTCDA and Pt on top of YIG.

In our SP measurements, a TE_{102} resonant cavity is used to apply 9.75 GHz microwaves to the devices. Figure 1 shows the setup of the SP measurements for microwave absorption spectra and corresponding V_{ISHE}. The mechanism of SP mainly correlates with magnetization dynamics, which could be expressed by the Landau–Lifshitz–Gilbert (LLG) equation $\mathrm{d}\hat{\boldsymbol{m}}/\mathrm{d}t = -|\gamma|(1+\alpha^2)\hat{\boldsymbol{m}} \times \boldsymbol{H}_{\mathrm{eff}} + \alpha\hat{\boldsymbol{m}} \times \mathrm{d}\hat{\boldsymbol{m}}/\mathrm{d}t$, where $\hat{\boldsymbol{m}}$ is a unit vector of the magnetization, $\boldsymbol{H}_{\mathrm{eff}}$ is an effective magnetic field, and α is the dimensionless Gilbert damping constant.[26,27] By assuming that $\boldsymbol{H}_{\mathrm{eff}}$ contains a demagnetizing field induced by shape anisotropy, $\boldsymbol{H}_{\mathrm{eff}} = \boldsymbol{H}_{\mathrm{dc}} + \boldsymbol{h}_{\mathrm{ac}}(t) = h_x \exp[i\omega t]\hat{\mathbf{i}} + (h_y \exp[i\omega t] - M_y(t))\hat{\mathbf{j}} + H\hat{\mathbf{k}}$ with undamped oscillatory solutions, a dynamic Polder susceptibility tensor $\boldsymbol{\chi}(\omega)$ in our thin film systems could be acquired,[28–30]

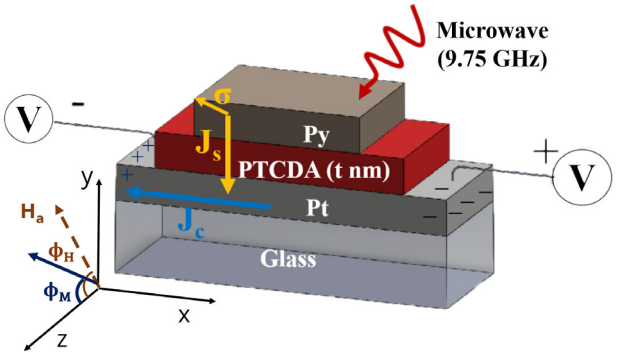

FIG. 1. A schematic illustration of SP devices. ϕ_H and ϕ_M represent the angle of the static external magnetic field H and the magnetization. After a 9.75 GHz microwave is applied, a spin current J_s with spin σ will be pumped into PTCDA from Py. J_s reaching Pt will be converted to a charge current J_c by the ISHE.

$$\begin{bmatrix} \chi_{xx} & \chi_{xy} \\ \chi_{yx} & \chi_{yy} \end{bmatrix} = \frac{\omega_M}{(\omega_H + i\alpha\omega)(\omega_H + \omega_M + i\alpha\omega) - \omega^2} \times \begin{bmatrix} \omega_H + \omega_M + i\alpha\omega & i\omega_M \\ -i\omega & \omega_H + i\alpha\omega \end{bmatrix}, \quad (1)$$

where ω is the angular frequency of the microwave, $\omega_H = |\gamma|H$, and $\omega_M = |\gamma|M_s$ from the saturation magnetization M_s. Based on Poynting's theorem,[31] Maxwell equations, and $\boldsymbol{\chi}$ in Eq. (1), time-average power absorbed in the TE_{102} resonant cavity with the ac magnetic field in the x-direction could be derived,[32]

$$\begin{aligned} \langle P \rangle_t &= -\int_V \langle i\omega \boldsymbol{h}_{\mathrm{ac}} \cdot (\mathbb{1} + \boldsymbol{\chi}) \cdot \boldsymbol{h}_{\mathrm{ac}} \rangle_t d\tau \\ &= \frac{1}{2}\omega h_x^2 V \mathrm{Im}(\chi_{xx}^*) \\ &= \frac{h_x^2 V}{2} \frac{\gamma M_s (H + M_s)}{\alpha(2H + M_s)} \frac{\Delta H^2}{(H - H_0)^2 + \Delta H^2}, \end{aligned} \quad (2)$$

where V is the volume of the ferromagnetic layer, $\boldsymbol{e}$ is an electric field inside, and 1 is an identity matrix. $\mathrm{Im}(\chi_{xx})$ results in a Lorentz line shape of the absorption spectra with a linewidth $\Delta H = \alpha\omega(2H + M_s) \times [\gamma(H_0 + H + M_s)]^{-1}$, and the field H_0 satisfies a resonance condition of the magnetic thin film:[32] $\omega = (\omega_H(\omega_H + \omega_M))^{1/2}$. As shown above, $\boldsymbol{\chi}$ not only demonstrates a phase shift between the magnetization and the external magnetic field but also strongly correlates with the line shape of effects induced by spin dynamics. The absorption spectrum of the 15-nm-PTCDA SP device is fitted with Eq. (2) with characteristic strength $I = h_x^2 V \gamma M_s (H + M_s)[\alpha(4H + 2M_s)]^{-1}$, shown in Fig. 2(a). The ultrathin Py layers forbid the creation of spin waves and allow only the uniform-mode ferromagnetic resonance,

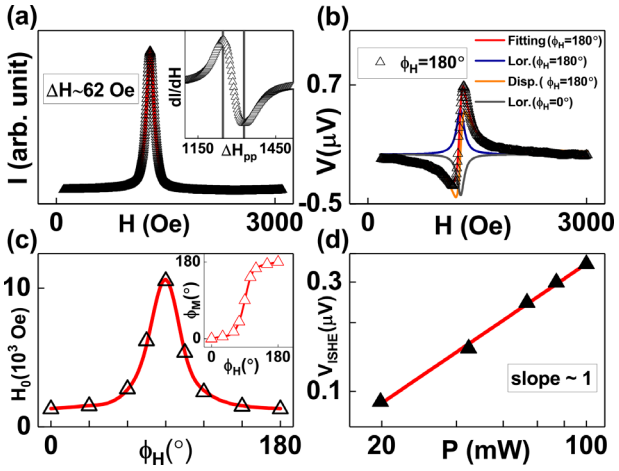

FIG. 2. (a) An absorption spectrum of Pt/15 nm PTCDA/Py with $\phi_H = 180^\circ$ is plotted as a function of the applied field H. Line shape could be described by Eq. (2) with $\Delta H \sim 62$ Oe and $H_0 \sim 1278$ Oe. The fitted curve is represented by a red line. The inset is a derivative absorption spectrum that gives peak-to-peak linewidth $\Delta H_{\mathrm{pp}} \sim 70$ Oe, which agrees with the relation $\Delta H = 2\Delta H_{\mathrm{pp}}/\sqrt{3}$. (b) Field-dependent voltage with $\phi_H = 180^\circ$ and the fitting curves. The resonance field is similar with that in the absorption spectrum in (a). (c) Angle-dependent resonance field and the fitted curve. Inset: plot of ϕ_M vs ϕ_H. (d) A linear relation between V_{ISHE} and microwave power P is verified.

resulting in the only one peak in the absorption spectrum.[32] The fact that $V(H)$ in Fig. 2(b) and the absorption spectra share the same resonance fields implies that the voltage signals originate from SP and the spin rectification (SR) effects.

Field-dependent voltage of devices within the cavity could be expressed as[24]

$$V(H) = V_s \frac{\Delta H^2}{(H-H_0)^2+\Delta H^2} + V_a \frac{-2(H-H_0)\Delta H}{(H-H_0)^2+\Delta H^2}. \quad (3)$$

Proportional to the microwave absorption, V_{ISHE} is in the form a Lorentzian line shape and contributes to the symmetric term V_s, while V_a originates from the SR effects.[15,33–35] By fitting Eq. (3) to the results, we acquired V_s and V_a around 0.45 and −0.43 μV in the 15-nm PTCDA device with a microwave power of 100 mW, shown in Fig. 2(b). Sign inversion of the fitted V_s at $\phi_H = 0°$ and 180° in Fig. 2(b) is consistent with the ISHE. Angle-dependent H_0 in Fig. 2(c) can be described by Kittel's formula,[36,37] revealing a saturation magnetization $4\pi M_s$ of around 7200 Gauss as well as a gyromagnetic ratio $|\gamma/2\pi|$ of 2.90×10^6 Hz/Gauss. Figure 2(d) also verifies a linear relation between the ISHE voltage and power:[33] $V_{\mathrm{ISHE}} \propto h^2 \propto P$. These repeatable results show stability of the devices and confirm V_{ISHE} is induced by SP.

The spin diffusion length of PTCDA, λ_s, can be extracted from the exponential decay of V_{ISHE}, which is proportional to $\exp[-t/\lambda_s]$ with t being the thickness of the PTCDA layer.[15,16,38] However, to discuss such spin transport in devices with varied t, V_{ISHE} needs to be carefully normalized. The time-average dc spin currents injected into PTCDA can be described by exchange interaction between conduction electrons and local moments,[27]

$$j_s^0(H) = \frac{\hbar}{2} g_{\mathrm{eff}}^{\uparrow\downarrow} \frac{\omega}{2\pi} \frac{h_x^2}{2M_s^2} \mathrm{Im}(-\chi_{xx}^* \chi_{yx} + \chi_{yx}^* \chi_{xx})$$

$$= \frac{1}{4} \frac{\hbar}{2} g_{\mathrm{eff}}^{\uparrow\downarrow} \frac{h_x^2 \gamma \sqrt{H(H+M_s)}}{2\pi[(H-H_0)^2+\Delta H^2]} \quad (4a)$$

$$= \frac{\hbar}{2} g_{\mathrm{eff}}^{\uparrow\downarrow} \frac{h_x^2 \gamma (H+M_s)}{2\pi\alpha^2(2H+M_s)^2} \frac{\Delta H^2}{(H-H_0)^2+\Delta H^2}, \quad (4b)$$

where $g_{\mathrm{eff}}^{\uparrow\downarrow}$ is the effective spin mixing conductance. The damping constant α can be separated into an intrinsic α_0 and an additional α'. The latter is proportional to $g_{\mathrm{eff}}^{\uparrow\downarrow}$: $\alpha' = |\gamma|\hbar(4\pi M_s V)^{-1} g_{\mathrm{eff}}^{\uparrow\downarrow}$. In t-dependent measurements, $g_{\mathrm{eff}}^{\uparrow\downarrow}$ depends on the spin back flow from PTCDA and can be expressed as[27]

$$g_{\mathrm{eff}}^{\uparrow\downarrow}(t) = \left[1 + \frac{g_1^{\uparrow\downarrow}}{g} \frac{1+\tanh(t/\lambda_s) g_2^{\uparrow\downarrow}/g}{\tanh(t/\lambda_s) + g_2^{\uparrow\downarrow}/g}\right]^{-1} g_1^{\uparrow\downarrow},$$

where g is the spin conductance in PTCDA per λ_s, and $g_1^{\uparrow\downarrow}$ and $g_2^{\uparrow\downarrow}$ are $g^{\uparrow\downarrow}$ at the Py–PTCDA and PTCDA–Pt interfaces, respectively. Although the change of $g_{\mathrm{eff}}^{\uparrow\downarrow}$ with t directly affects j_s^0 and corresponding V_{ISHE}, it is irrelevant to spin scattering in PTCDA and should be removed by dividing α' into V_{ISHE}. h_x in Eqs. (4) depends on the power of microwave in resonance cavity and could slightly deviate after device replacements, which can be eliminated by normalization over the absorption strength I. In addition, comparing the Lorentzian expression in Eqs. (3) and (4b) with the original form of $j_s^0 \propto 1/[(H-H_0)^2 + \Delta H^2]$ in Eq. (4a), one notices that an additional ΔH^2 should be included in V_{ISHE} to compensate the mathematical input for Lorentzian fitting. Since I already contains ΔH in its denominator, only ΔH to the power of one needs to be involved. Hence, we introduce a normalized ISHE voltage, $\tilde{V}_{\mathrm{ISHE}} = V_{\mathrm{ISHE}} \Delta H (I\alpha')^{-1}$, by removing the change of $g_{\mathrm{eff}}^{\uparrow\downarrow}$ in each device, the variation of h_x in the cavity, and the mathematical input. After the normalization, a variation of $\tilde{V}_{\mathrm{ISHE}}$ among the devices is contributed solely by spin transport in PTCDA. In Fig. 3, $\tilde{V}_{\mathrm{ISHE}}$ is plotted as a function of PTCDA thickness t. To bring data to the same scale for comparisons, $\tilde{V}_{\mathrm{ISHE}}$ is divided by $\tilde{V}_{\mathrm{ISHE}}$(1 nm) and $\tilde{V}_{\mathrm{ISHE}}$(5 nm) in Figs. 3(a) and 3(b), respectively. In the thinner t region [<5 nm, gray zone in Fig. 3(a)], an abnormal enhancement of $\tilde{V}_{\mathrm{ISHE}}$ is observed, which will be discussed later. In the thicker t region [≥ 5 nm, white zone in Fig. 3(a)], $\tilde{V}_{\mathrm{ISHE}}$ exponentially decays as expected. Figure 3(b) shows a fitted curve of data in the white zone with λ_s of 11.48 ± 0.08 nm, which is of the same order of magnitude as the previous study.[25] Insets of Figs. 3(a) and 3(b) show the data without normalization by $\Delta H(I\alpha')^{-1}$. λ_s obtained from unnormalized V_{ISHE} is 16 ± 2 nm, and the residual sum of squares is three orders of magnitude larger. While resistivity of Pt, dimensional parameters, and the temperature dependency of spin diffusion length may also disturb the SP measurements, they were well-controlled in our SP devices. Pt resistivity around 30.6 $\mu\Omega$ cm is deduced from direct I–V measurements and is stable from sample to sample. Despite fruitful works of spin transport in organic molecules in previous studies,[15,25,34,35,38–40] normalization other than dividing spin-detector resistance has not been fully elaborated. The much improved λ_s precision by our developed normalization method proves the method effective. Addressing the instability of spin sources, the normalization method is not limited to organic spacer and can be generally applied to SP devices with similar structures. It is also worth noting that recent studies point out that SR effects could contribute to both V_s and V_a in spin pumping voltage, depending on electromagnetic phase Φ.[41,42] Detailed angular-dependent experiments for the extraction of Φ should help to improve accuracy of λ_s from SP studies.

The injection of spin currents into PTCDA by the LSSE was performed by creating a temperature gradient of 8 K between the top and bottom surfaces in YIG/PTCDA(t nm)/Pt, as shown in Fig. 4. V_{ISHE} induced by the LSSE in a device without PTCDA (i.e., YIG/Pt) is comparable to that induced by SP in Pt/Py [Figs. 5(a) and 5(b)]. A plateau

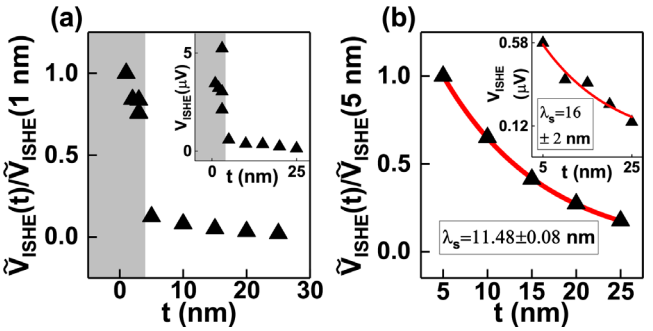

FIG. 3. (a) Thickness-dependence of the normalized ISHE voltage $\tilde{V}_{\mathrm{ISHE}}$. An abnormal enhancement of magnitude is observed in a gray region. The inset in (a) displays V_{ISHE} before the normalization. (b) A spin diffusion length of 11.48 ± 0.08 nm is acquired by fitting an exponential decay to normalized thickness-dependent $\tilde{V}_{\mathrm{ISHE}}$ in the white region. Unnormalized data in the inset in (b) give a spin diffusion length of 16 ± 2 nm.

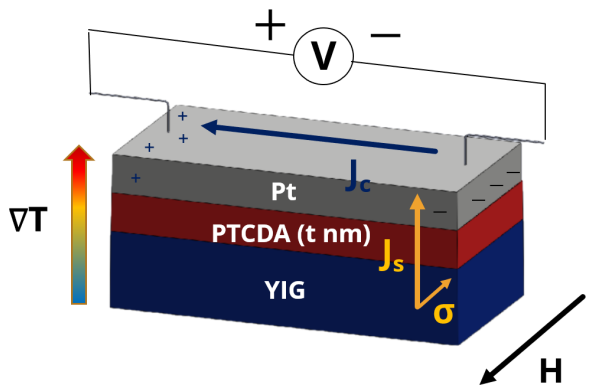

FIG. 4. A diagrammatic sketch of the LSSE in a device. Dimensions of the substrate YIG are 2 mm × 5 nm. A temperature difference between top and bottom of the devices is 8 K, measured by thermal couples.

behavior shown in Fig. 5(a) is caused by a non-collinear magnetization configuration between the surface and bulk of YIG.[43] In the thickness-dependent LSSE results in Fig. 5(c), V_{ISHE} is not detectable if the thickness of PTCDA is larger than ∼4.5 nm, which differs from the SP results. No matter in SP or the LSSE, mechanisms of spin current generation are associated mainly with interface spin-exchange interaction, of which the strength is correlated with $g^{\uparrow\downarrow}$, between local moments and conduction electrons.[27,44,45] Spin injection efficiencies are utterly disparate when inserting PTCDA, even though spin injection efficiency of the pristine Py-based SP system is similar to that of the pristine YIG-based LSSE devices, shown in Figs. 5(a) and 5(b). This phenomenon suggests that $g^{\uparrow\downarrow}$ is extremely reduced at YIG/PTCDA interfaces compared to that at the Py/PTCDA interface. Interfacial hybridization of the electron orbits between OSCs and metals correlates with spin behaviors and might play an important role here.[10,46] In our previous work of organic spin valves, we have unveiled hybrid states between PTCDA and metals by x-ray photoelectron spectroscopy.[47] The single-bond oxygen atoms in PTCDA have a strong chemical interaction with adjacent metal atoms, which leads to hybridization and extra spin-flip scattering. In related studies, high density of states within PTCDA bandgap induced by reactive metals are observed and calculated as well.[48–50] The insertion of a partially oxidized layer Al_xO could suppress the hybrid states and preserve the spin injection by bias voltage.[14,47,51–54] The oxide insertion is, however, not necessary in SP as shown in Fig. 2. This contrast indicates that the hybrid states suppress electrical spin injection[10] but allow exchange interaction for SP by offering more conduction electrons. On the other hand, the wide bandgap of YIG could forbid the formation of YIG–PTCDA hybrid states and, thus, lead to reduced $g^{\uparrow\downarrow}$ and vanishing V_{ISHE}. Accordingly, the spin injection efficiency depends on the hybrid states at the OSC/ferromagnet interface, and, therefore, materials with the higher density of hybrid states in between could be selected to enhance the spin injection efficiency.

As in the Py–PTCDA systems, high V_{ISHE} appears in the YIG–PTCDA devices when PTCDA is thin [gray regions in Figs. 3(a) and 5(c)]. To address origins of the sudden increase in V_{ISHE}, the temperature-dependent LSSE measurements were performed with 3 nm PTCDA. The temperature dependence of the LSSE in YIG-based systems can be described by the bulk magnon chemical potential theory[44] and an atomistic spin model,[55,56] which is described in detail in the supplementary material. As mentioned in Ref. 56, the peak position strongly depends on the interface effects. In Fig. 6(a), the trend

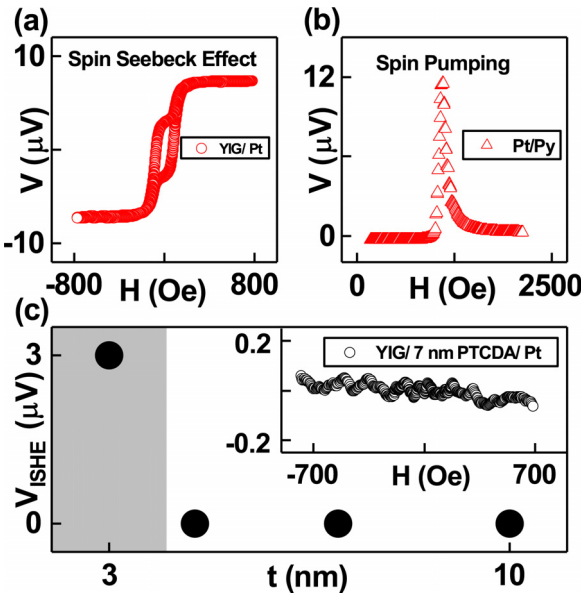

FIG. 5. (a) and (b) are H-dependent voltage measurements of the LSSE and SP, respectively. Magnitudes of V_{ISHE} induced by two distinct effects are comparable. (c) Thickness-dependent LSSE measurements show V_{ISHE} vanishes after the insertion of 4.5 nm and thicker PTCDA. Note that the boundary between gray and white is not definite. The inset shows disappearance of V_{ISHE} with 7 nm PTCDA.

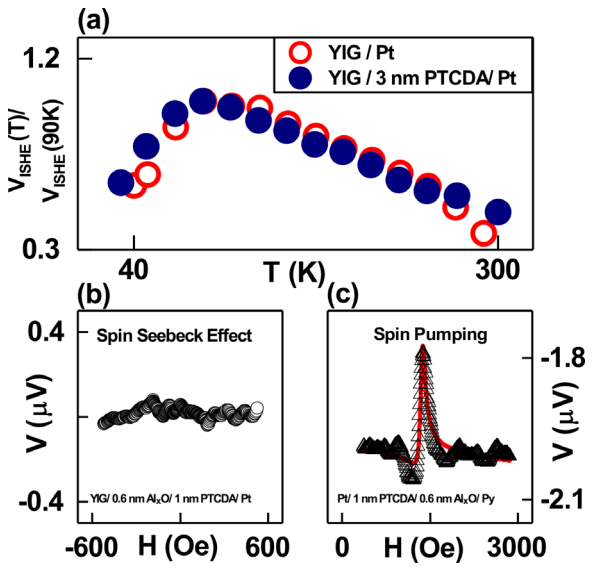

FIG. 6. (a) Trends of temperature-dependent V_{ISHE} induced by LSSE are similar before and after the insertion of a 3 nm PTCDA spacer. (b) and (c) are V_{ISHE} from the LSSE and SP, respectively. Spin currents pass through a hybrid spacer, composed of a partially oxidized aluminum layer and PTCDA, in series of SP but are blocked in the LSSE measurements. V_{ISHE} induced by SP is around 0.20 μV.

resembles that of pristine YIG/Pt sample with no obvious peak shift, which implies potential pinhole issues in the gray regions. The indication is reasonable since the arithmetic mean deviation roughness of PTCDA is about 1.39 nm for both the SP and LSSE systems. Therefore, the abnormally large V_{ISHE} in the thin (gray) regions in both the SP and LSSE measurements can be attributed to pinholes from the top Py and Pt layers, respectively. Several studies of organic spin valves have demonstrated that Al-oxide would reduce the impact of pinholes and enhance spin injection into the organic layers.[57,58] In our previous work, it has been shown that the junction conductance G_J decreases exponentially with the PTCDA thickness when an Al_xO layer is inserted, and a reasonable extinction coefficient β is obtained by fitting G_J with $G_0 \exp[-\beta t]$, indicating that the junctions are pinhole-free.[14] To block direct contact through pinholes, we inserted Al_xO into YIG/PTCDA and PTCDA/Py with 1-nm PTCDA. After the Al_xO insertion, V_{ISHE} in Figs. 6(b) and 6(c) is comparable to those in the thick PTCDA regions in Figs. 5(c) and 3(a), respectively, which support our speculation about pinhole-induced large V_{ISHE} in the thin PTCDA devices.

It should be noted that, in the Py-based devices, V_{ISHE} (1 nm PTCDA/0.6 nm Al_xO) is close to V_{ISHE}(25 nm PTCDA), as shown in Fig. 6(c) and the inset of Fig. 3(b). Since V_{ISHE} of the device with the insertion of 0.6 nm Al_xO is comparable with that in pristine Pt/Py devices (data not shown), the significant drop of V_{ISHE} is not caused by spin transport in Al_xO. As mentioned in the previous paragraphs, Al_xO can suppress hybrid states and the corresponding conduction electrons, which benefit SP. We conclude that Al_xO restrains Py–PTCDA hybridization and, therefore, reduces the spin injection efficiency. On the other hand, the PTCDA–Pt interfaces could affect the spin transport by extra spin-flip scattering induced from interdiffusion,[10,59] which might occur in our LSSE devices due to the fabrication sequence. To clarify this issue, we fabricated a reversed Py-based SP device (Py/Al_xO/PTCDA/Pt). V_{ISHE} from the reversed device has similar order of magnitude to the original structure, indicative of subtle change in the spin transport efficiency at the PTCDA–Pt interfaces with and without Pt interdiffusion (see the supplementary material for the SP result). Namely, the poor spin injection efficiency in the LSSE devices is not caused by the interdiffusion at the PTCDA–Pt interfaces.

In summary, the experiments of spin injection into PTCDA by SP and the LSSE are performed. Distinct V_{ISHE} acquired predicts significant reduction of $g^{\uparrow\downarrow}$ at the YIG–PTCDA interfaces compared to that at the Py–PTCDA interfaces. A normalization factor has been introduced to our SP system and disposes of V_{ISHE} deviations caused by the spin sources, which leads to a more precise λ_s. The role of hybrid states in spin injection efficiency depends on material choices and the injection method. Our qualitative characterization of $g^{\uparrow\downarrow}$ in the present work points out the importance of organic interfaces in spin injection, which is worth of further endeavor.

See the supplementary material for the morphological profiles of the PTCDA films and the SP measurement of the reversed Py-based device.

This work was supported by the Ministry of Science and Technology (MOST) of Taiwan under Grant No. 107-2119-M-002-006.

AUTHOR DECLARATIONS

Conflict of Interest

The authors have no conflicts to disclose.

Author Contributions

Sheng-Yueh Weng: Formal analysis (lead); Investigation (lead); Writing – original draft (equal); Writing – review & editing (equal). **Minn-Tsong Lin:** Conceptualization (lead); Funding acquisition (lead); Methodology (equal); Supervision (lead); Writing – original draft (equal); Writing – review & editing (equal). **M. Sanjoy Singh:** Formal analysis (supporting); Investigation (supporting). **Cheng-Feng Hong:** Investigation (supporting). **Wen-Teng Lin:** Formal analysis (supporting); Investigation (supporting). **Po-Hsun Wu:** Resources (equal). **Ssu-Yen Huang:** Methodology (equal); Resources (equal). **J. G. Lin:** Methodology (equal); Resources (equal). **Yu-Hsun Chu:** Formal analysis (supporting); Writing – review & editing (equal). **Wen-Chung Chiang:** Writing – review & editing (equal).

DATA AVAILABILITY

The data that support the findings of this study are available from the corresponding author upon reasonable request.

REFERENCES

[1]J. Devkota, R. Geng, R. C. Subedi, and T. D. Nguyen, Adv. Funct. Mater. **26**, 3881 (2016).
[2]W. Xu, G. J. Szulczewski, P. LeClair, I. Navarrete, R. Schad, G. Miao, H. Guo, and A. Gupta, Appl. Phys. Lett. **90**, 072506 (2007).
[3]V. A. Dediu, L. E. Hueso, I. Bergenti, and C. Taliani, Nat. Mater. **8**, 707 (2009).
[4]T. D. Nguyen, E. Ehrenfreund, and Z. V. Vardeny, Science **337**, 204 (2012).
[5]M. Cinchetti, K. Heimer, J.-P. Wüstenberg, O. Andreyev, M. Bauer, S. Lach, C. Ziegler, Y. Gao, and M. Aeschlimann, Nat. Mater. **8**, 115 (2009).
[6]A. J. Drew, J. Hoppler, L. Schulz, F. L. Pratt, P. Desai, P. Shakya, T. Kreouzis, W. P. Gillin, A. Suter, N. A. Morley, V. K. Malik, A. Dubroka, K. W. Kim, H. Bouyanfif, F. Bourqui, C. Bernhard, R. Scheuermann, G. J. Nieuwenhuys, T. Prokscha, and E. Morenzoni, Nat. Mater. **8**, 109 (2009).
[7]H. Isshiki, K. Kondou, S. Takizawa, K. Shimose, T. Kawabe, E. Minamitani, N. Yamaguchi, F. Ishii, A. Shiotari, Y. Sugimoto, S. Miwa, and Y. Otani, Nano Lett. **19**, 7119 (2019).
[8]H. Nakayama, T. Yamamoto, H. An, K. Tsuda, Y. Einaga, and K. Ando, Sci. Adv. **4**, eaar3899 (2018).
[9]K. V. Raman, S. M. Watson, J. H. Shim, J. A. Borchers, J. Chang, and J. S. Moodera, Phys. Rev. B **80**, 195212 (2009).
[10]C. Barraud, P. Seneor, R. Mattana, S. Fusil, K. Bouzehouane, C. Deranlot, P. Graziosi, L. Hueso, I. Bergenti, V. Dediu, F. Petroff, and A. Fert, Nat. Phys. **6**, 615 (2010).
[11]F. J. Yue, Y. J. Shi, B. B. Chen, H. F. Ding, F. M. Zhang, and D. Wu, Appl. Phys. Lett. **101**, 022416 (2012).
[12]J. H. Shim, K. V. Raman, Y. J. Park, T. S. Santos, G. X. Miao, B. Satpati, and J. S. Moodera, Phys. Rev. Lett. **100**, 226603 (2008).
[13]G. Szulczewski, H. Tokuc, K. Oguz, and J. M. D. Coey, Appl. Phys. Lett. **95**, 202506 (2009).
[14]K.-S. Li, Y.-M. Chang, S. Agilan, J.-Y. Hong, J.-C. Tai, W.-C. Chiang, K. Fukutani, P. A. Dowben, and M.-T. Lin, Phys. Rev. B **83**, 172404 (2011).
[15]S. Watanabe, K. Ando, K. Kang, S. Mooser, Y. Vaynzof, H. Kurebayashi, E. Saitoh, and H. Sirringhaus, Nat. Phys. **10**, 308 (2014).
[16]S. W. Jiang, S. Liu, P. Wang, Z. Z. Luan, X. D. Tao, H. F. Ding, and D. Wu, Phys. Rev. Lett. **115**, 086601 (2015).
[17]V. Kalappattil, R. Geng, R. Das, M. Pham, H. Luong, T. Nguyen, A. Popescu, L. M. Woods, M. Kläui, H. Srikanth, and M. H. Phan, Mater. Horiz. **7**, 1413 (2020).

[18]S. Kowarik, A. Gerlach, and F. Schreiber, J. Phys. Condens. Matter. **20**, 184005 (2008).
[19]N. R. Armstrong, W. Wang, D. M. Alloway, D. Placencia, E. Ratcliff, and M. Brumbach, Macromol. Rapid Commun. **30**, 717 (2009).
[20]G.-H. Cao, D.-S. Qin, M. Guan, J.-S. Cao, Y.-P. Zeng, and J.-M. Li, Chin. Phys. Lett. **24**, 1380 (2007).
[21]O. Mosendz, J. E. Pearson, F. Y. Fradin, G. E. W. Bauer, S. D. Bader, and A. Hoffmann, Phys. Rev. Lett. **104**, 046601 (2010).
[22]K. Uchida, H. Adachi, T. Ota, H. Nakayama, S. Maekawa, and E. Saitoh, Appl. Phys. Lett. **97**, 172505 (2010).
[23]J. E. Hirsch, Phys. Rev. Lett. **83**, 1834 (1999).
[24]E. Saitoh, M. Ueda, H. Miyajima, and G. Tatara, Appl. Phys. Lett. **88**, 182509 (2006).
[25]K. Nishida, Y. Teki, and E. Shikoh, Solid State Commun. **312**, 113898 (2020).
[26]T. L. Gilbert, IEEE Trans. Magn. **40**, 3443 (2004).
[27]Y. Tserkovnyak, A. Brataas, and G. E. W. Bauer, Phys. Rev. B **66**, 224403 (2002).
[28]J. Xiao, "Spin Seebeck effect," in *Spintronics for Next Generation Innovative Devices* (Wiley, 2015), Chap. 7, p. 125.
[29]M. Harder, Y. Gui, and C.-M. Hu, Phys. Rep. **661**, 1 (2016).
[30]R. Iguchi and E. Saitoh, J. Phys. Soc. Jpn. **86**, 011003 (2017).
[31]J. H. Poynting, Philos. Trans. R. Soc. London **175**, 343 (1884).
[32]C. Kittel, *Introduction to Solid State Physics* (Wiley, 2004), Chap. 13, p. 361.
[33]K. Ando, S. Takahashi, J. Ieda, Y. Kajiwara, H. Nakayama, T. Yoshino, K. Harii, Y. Fujikawa, M. Matsuo, S. Maekawa, and E. Saitoh, J. Appl. Phys. **109**, 103913 (2011).
[34]Z. Li, T. Li, D.-C. Qi, W. Tong, L. Xu, J. Zhu, Z. Zhang, H. Xu, W. Zhang, Y. Guo, F. Chen, Y. Han, L. Cao, F. Zhang, and Y. Xiong, Appl. Phys. Lett. **115**, 053301 (2019).
[35]H. Liu, J. Wang, A. Chanana, and Z. V. Vardeny, J. Appl. Phys. **125**, 142908 (2019).
[36]J. Lindner, I. Barsukov, C. Raeder, C. Hassel, O. Posth, R. Meckenstock, P. Landeros, and D. L. Mills, Phys. Rev. B **80**, 224421 (2009).
[37]S. Mizukami, Y. Ando, and T. Miyazaki, Phys. Rev. B **66**, 104413 (2002).
[38]Y. Tani, Y. Teki, and E. Shikoh, Appl. Phys. Lett. **107**, 242406 (2015).
[39]H. Liu, J. Wang, M. Groesbeck, X. Pan, C. Zhang, and Z. V. Vardeny, J. Mater. Chem. C **6**, 3621 (2018).
[40]M. Kimata, D. Nozaki, Y. Niimi, H. Tajima, and Y. Otani, Phys. Rev. B **91**, 224422 (2015).
[41]J. Lustikova, Y. Shiomi, and E. Saitoh, Phys. Rev. B **92**, 224436 (2015).
[42]P. Skalski, O. Zadvorna, D. Venkateshvaran, and H. Sirringhaus, Phys. Rev. Mater. **6**, 024601 (2022).
[43]P.-H. Wu and S.-Y. Huang, Phys. Rev. B **94**, 024405 (2016).
[44]L. J. Cornelissen, K. J. H. Peters, G. E. W. Bauer, R. A. Duine, and B. J. van Wees, Phys. Rev. B **94**, 014412 (2016).
[45]S. M. Rezende, R. L. Rodríguez-Suárez, R. O. Cunha, J. C. López Ortiz, and A. Azevedo, J. Magn. Magn. Mater. **400**, 171 (2016).
[46]Y.-H. Chu, C.-H. Hsu, C.-I. Lu, H.-H. Yang, T.-H. Yang, C.-H. Luo, K.-J. Yang, S.-H. Hsu, G. Hoffmann, C.-C. Kaun, and M.-T. Lin, ACS Nano **9**, 7027 (2015).
[47]J.-Y. Hong, K.-H. Ou Yang, B.-Y. Wang, K.-S. Li, H.-W. Shiu, C.-H. Chen, Y.-L. Chan, D.-H. Wei, F.-H. Chang, H.-J. Lin, W.-C. Chiang, and M.-T. Lin, Appl. Phys. Lett. **104**, 083301 (2014).
[48]I. Hill, D. Milliron, J. Schwartz, and A. Kahn, Appl. Surf. Sci. **166**, 354 (2000).
[49]Y. Hirose, A. Kahn, V. Aristov, P. Soukiassian, V. Bulovic, and S. R. Forrest, Phys. Rev. B **54**, 13748 (1996).
[50]S. Picozzi, A. Pecchia, M. Gheorghe, A. Di Carlo, P. Lugli, B. Delley, and M. Elstner, J. Comput. Electron. **2**, 407 (2003).
[51]J.-Y. Hong, S.-H. Chen, W.-C. Chiang, and M.-T. Lin, Spin **04**, 1440015 (2014).
[52]J. P. Cascales, J.-Y. Hong, I. Martinez, M.-T. Lin, T. Szczepański, V. K. Dugaev, J. Barnaś, and F. G. Aliev, Appl. Phys. Lett. **105**, 233302 (2014).
[53]T. Szczepański, V. K. Dugaev, J. Barnaś, I. Martinez, J. P. Cascales, J.-Y. Hong, M.-T. Lin, and F. G. Aliev, Phys. Rev. B **94**, 235429 (2016).
[54]I. Martinez, J. P. Cascales, C. Gonzalez-Ruano, J.-Y. Hong, C.-F. Hung, M.-T. Lin, T. Frederiksen, and F. G. Aliev, J. Phys. Chem. C **122**, 26499 (2018).
[55]A. Kehlberger, U. Ritzmann, D. Hinzke, E.-J. Guo, J. Cramer, G. Jakob, M. C. Onbasli, D. H. Kim, C. A. Ross, M. B. Jungfleisch, B. Hillebrands, U. Nowak, and M. Kläui, Phys. Rev. Lett. **115**, 096602 (2015).
[56]E.-J. Guo, J. Cramer, A. Kehlberger, C. A. Ferguson, D. A. MacLaren, G. Jakob, and M. Kläui, Phys. Rev. X **6**, 031012 (2016).
[57]X. Zhang, S. Mizukami, T. Kubota, Q. Ma, M. Oogane, H. Naganuma, Y. Ando, and T. Miyazaki, Nat. Commun. **4**, 1392 (2013).
[58]T. L. A. Tran, T. Q. Le, J. G. M. Sanderink, W. G. van der Wiel, and M. P. de Jong, Adv. Funct. Mater. **22**, 1180 (2012).
[59]I. Žutić, J. Fabian, and S. Das Sarma, Rev. Mod. Phys. **76**, 323 (2004).